Journal of Computational Physics 228 (2009) 6784–6795

Contents lists available at ScienceDirect

Journal of Computational Physics

journal homepage: www.elsevier.com/locate/jcp

Phase-field simulation of microstructure formation in technical castings – A self-consistent homoenthalpic approach to the micro–macro problem

B. Böttger *, J. Eiken, M. Apel

ACCESS e.V., RWTH Aachen, Intzestraße 5, 52072 Aachen, Germany

ARTICLE INFO

Article history:
Received 17 February 2009
Received in revised form 25 May 2009
Accepted 5 June 2009
Available online 30 June 2009

PACS:
81.30.Fb
44.05.+e
07.05.Tp
02.70.Bf

Keywords:
Equiaxed microstructure
Solidification
Phase-field modeling
Grain size
Casting
Multi-scale model

ABSTRACT

Performing microstructure simulation of technical casting processes suffers from the strong interdependency between latent heat release due to local microstructure formation and heat diffusion on the macroscopic scale: local microstructure formation depends on the macroscopic heat fluxes and, in turn, the macroscopic temperature solution depends on the latent heat release, and therefore on the microstructure formation, in all parts of the casting. A self-consistent homoenthalpic approximation to this micro–macro problem is proposed, based on the assumption of a common enthalpy–temperature relation for the whole casting which is used for the description of latent heat production on the macroscale. This enthalpy–temperature relation is iteratively obtained by phase-field simulations on the microscale, thus taking into account the specific morphological impact on the latent heat production.

This new approach is discussed and compared to other approximations for the coupling of the macroscopic heat flux to complex microstructure models. Simulations are performed for the binary alloy Al–3at%Cu, using a multiphase-field solidification model which is coupled to a thermodynamic database. Microstructure formation is simulated for several positions in a simple model plate casting, using a one-dimensional macroscopic temperature solver which can be directly coupled to the microscopic phase-field simulation tool.

1. Introduction

In technical casting processes, microstructure formation is inherently linked to the macroscopic heat flow. This fact has a strong impact on the simulation of technical castings, because both length-scales, the microscopic scale of the phase transformation processes and the macroscopic scale of heat conduction, have to be considered simultaneously. A rigorous coupling of the two length-scales is computationally very ambitious.

If the main interest lies in the macroscopic scale, a viable pragmatic approach is the use of very simple microstructure models which are still exact enough within the scope of the macroscopic problem. Essentially, dedicated heat flow models for technical solidification processes only need a proper description of the latent heat caused by the phase transformation. For industrial applications, in most cases, no exact information on the microstructure formation process is available, and heat flow simulation tools often use simplified latent heat descriptions based on DSC experiments or thermodynamic Scheil modeling. More elaborate microstructure models allow for an improvement of the heat flow prediction and, at the same time, they provide some microstructural information which might be of interest for material processing [1–4]. But this is only

* Corresponding author. Tel.: +49 241 8098008; fax: +49 241 38578.
E-mail address: B.Boettger@access.rwth-aachen.de (B. Böttger).
URL: http://www.access.rwth-aachen.de (B. Böttger).

0021-9991/$ - see front matter © 2009 Elsevier Inc. All rights reserved.
doi:10.1016/j.jcp.2009.06.028

possible, if the models are still sufficiently simple to be solved simultaneously on all nodes of the heat flow simulation grid within reasonable calculation times.

On the other hand, if the main focus is microstructure formation as it is in this paper, then such simple microstructure models may not deliver enough details, and more complex methods like phase-field will be necessary. These models, which allow for a detailed spatially resolved description of the morphology, have been widely applied to alloy solidification [5–8]. Due to the high computational effort which is inherent to those methods it is practically impossible to apply them simultaneously to all nodes of a heat flow grid – in many cases, microstructure simulation will be restricted to only one position. This raises the question of how the latent heat description can then be obtained for the other nodes, or, – and this is the focus of this article- in which way realistic thermal boundary conditions can be provided for complex microstructure modeling. Apart from special cases like directional solidification [9] or free growing dendrites [10], no general treatment of this problem, e.g. for equiaxed castings, has been published so far.

In this paper, a self-consistent homoenthalpic approximation is proposed for the problem at hand, which assumes a unique enthalpy–temperature relation for describing the latent heat release in all nodes. This relation is iteratively obtained from the simulation results, thereby consistently including the morphological aspects of solidification. Microscale simulation is performed on the basis of a multiphase-field model which is coupled to thermodynamic and diffusion databases and which has additionally been coupled to a macroscopic 1D temperature solver [11]. Unfortunately, a direct validation of the new approach is not possible due to the lack of experimental techniques for reproducible quantitative inoculation. Therefore, the homoenthalpic approach in this paper is applied to the solidification of the binary model system Al–3at%Cu in an equiaxed hypothetical plate casting in order to evaluate the applicability of the approach. A comparison to the "Bridgman" approach and the "DTA" approximation, which have been frequently used so far, is made, and the differences are discussed. The homoenthalpic approach finally is applied to the Al–3at%Cu casting, with the aim to predict the influence of different inoculation case scenarios on grain size and morphology in the Al–3at%Cu casting.

2. A multiphase-field model for technical alloys

The multiphase-field theory is a computational approach which describes the evolution of multiple phase-field parameters $\phi_\alpha(\vec{x},t)$ in time and space. These fields map the spatial distribution either of different grains of different orientation or of phases with different thermodynamic properties. At the interfaces, the phase-field variables change continuously between 0 and 1 over an interface thickness η which can be defined to be large compared to the atomic interface thickness but small compared to the microstructure length scale. The time evolution of the phases is calculated by a set of phase-field equations deduced by minimization of the free energy functional [8,12]:

$$\dot{\phi}_\alpha = \sum_\beta M_{\alpha\beta}(\vec{n})\left(\sigma^*_{\alpha\beta}(\vec{n})K_{\alpha\beta} + \frac{\pi}{\eta}\sqrt{\phi_\alpha\phi_\beta}\Delta G_{\alpha\beta}(\vec{c},T)\right) \tag{1}$$

$$K_{\alpha\beta} = \phi_\beta\nabla^2\phi_\alpha - \phi_\alpha\nabla^2\phi_\beta + \frac{\pi^2}{\eta^2}(\phi_\alpha - \phi_\beta) \tag{2}$$

In Eq. (1), $M_{\alpha\beta}$ is the mobility of the interface as a function of the interface orientation, described by the normal vector $\vec{n}$. $\sigma^*_{\alpha\beta}$ is the effective anisotropic surface energy (surface stiffness), and $K_{\alpha\beta}$ is related to the local curvature of the interface. The interface, on the one hand, is driven by the curvature contribution $\sigma^*_{\alpha\beta}K_{\alpha\beta}$ and on the other hand and by the thermodynamic driving force $\Delta G_{\alpha\beta}$. The thermodynamic driving force, which is a function of the local composition $\vec{c}$, couples the phase-field equations to the diffusion equations

$$\dot{\vec{c}} = \nabla\sum_{\alpha=1}^{N}\phi_\alpha\vec{D}_\alpha\nabla\vec{c}_\alpha \tag{3}$$

with $\vec{D}_\alpha$ being the multicomponent diffusion coefficient matrix for phase α. $\vec{D}_\alpha$ is calculated online for the given concentration and temperature by using the Fortran TQ interface to Thermo-Calc [13] and a mobility database [14].

2.1. Coupling to CALPHAD databases

Direct coupling to the thermodynamic database TTAL5 [15] via the Gibbs energy minimization software Thermo-Calc [13] is used. The thermodynamic driving force ΔG and the solute partitioning are calculated separately using the quasi-equilibrium approach [8], and introduced into the phase-field equation (Eq. (1)). This allows the software package to be independent of the specific thermodynamic data and not to be restricted by the number of elements or phases which are involved [11,16]. A multi-binary extrapolation scheme [8] was implemented to minimize the thermodynamic data handling, even for complex alloy systems [16]. Enthalpy data used by the temperature solver (Section 4) are also calculated by using the thermodynamic database.

3. The general micro–macro problem for castings

In molten metallic systems, temperature diffusion is about 10^3 or 10^4 times faster than solute diffusion. As a consequence, the diffusion fields for heat are much longer than those for the alloying elements dissolved in the melt, and solving both dif-

fusion equations on the same numerical grid is not efficient in most cases. Two models have to be used instead, one on the microscale and one on the macroscale, both depending on each other: The macro-model cannot work without the latent heat description provided by the microscale results, and the micro-model needs the thermal boundary conditions which is the output from the macroscale.

This general micro–macro problem has been treated in different ways, depending on the focus of the specific application. If emphasis is placed on the macroscopic scale, a frequently used method is to use the Scheil approximation or experimental DSC data as a basis for the description of the latent heat formation, and the dependency of latent heat on the local cooling conditions is neglected. Macroscopic simulation tools for casting typically allow specifying a global relation for the enthalpy or the fraction of solid versus temperature. More advanced approaches include microstructure models into the macroscopic heat flow model which are simple enough to be solved for all nodes of the macroscopic grid, but which are able to predict latent heat formation as a function of the local thermal conditions [3,4,17]. Those models can be regarded as a real solution of the general micro–macro problem, because full coupling between the scales is achieved. But they are restricted to simple microstructure models and often designed for special cases.

On the other hand, if microstructure prediction is the principle task as it is in most cases when the phase-field model is used, complete coupling can be excluded a priori as a possible solution of the micro–macro problem because of overly long simulation times. Consequently, in most publications on microstructure simulation using the phase-field method, the problem is avoided either by the use of extreme values for the temperature gradient [9] or by restriction to very small sample sizes [10]. These two approximations are discussed in the following, before the homoenthalpic approach is introduced in Section 3.3.

3.1. The Bridgman approximation

The Bridgman casting technique is designed to allow for precise experimental control over the thermal conditions during solidification. While in classical casting experiments the thermal gradient G is linked to the cooling rate $\overline{T}$ and the solidification velocity v, the Bridgman technique, via simultaneous heating and cooling, allows for making G and v independent. Furthermore, by making G as large a possible, the effect of latent heat can be minimized even for high values of v.

The Bridgman approximation for microstructure modeling more generally stands for applying an external temperature profile and neglecting the effects of latent heat. It has been widely used for the modeling of columnar dendritic growth and for the CET (columnar-to-equiaxed transition) [18–20], even without temperature gradient [21].

3.2. The DTA approximation

If the temperature gradient G is very small, latent heat can be considered to just raise the uniform temperature level of the simulation domain in competition with a uniform temperature drop due to an external heat extraction. This situation occurs experimentally, if cooling is extremely slow or if the sample size is small like in DTA and temperature gradients can be neglected. With this approximation, the global heat extraction per volume is the only thermal boundary condition of the micro-simulation domain which determines the local solidification time. According to the heat balance

$$\dot{q}dt = \frac{1}{V}\int_V \sum_\alpha d(H_\alpha \phi_\alpha) dV, \tag{4}$$

the global heat extraction per volume $\dot{q}$ is equal to the total enthalpy change in the system. H_α is the specific enthalpy of phase α, and ϕ_α the phase-field parameter, which is interpreted as the local phase fraction of phase α.

For application of the DTA approach in conjunction with the multiphase-field model which has been presented in Section 2, H_α has to be calculated in each time step for the whole micro-simulation domain by use of the Fortran TQ interface and the thermodynamic database. To reduce the numerical effort, the average phase fractions and phase compositions in the whole micro-simulation domain are calculated and used for obtaining H_α at the given temperature T. Consequently, conventional algorithms for determining the temperature change associated with release of latent heat like the enthalpy method where the temperature change dT is calculated indirectly via the total enthalpy change, cannot be used. Instead, in order to derive a direct explicit expression for dT, the enthalpy change in Eq. (4) is separated into three contributions: A temperature dependent term, corresponding to the heat capacity $c_{p,\alpha}$, a concentration dependent term caused by segregation or diffusion, and finally, the release of latent heat due to phase transformation:

$$d(H_\alpha \phi_\alpha) = \phi_\alpha \left(c_{p,\alpha} dT + \sum_k \frac{\partial H_\alpha}{\partial c_k} dc_k \right) + H_\alpha d\phi_\alpha \tag{5}$$

The temperature change dT can be calculated by extraction of the temperature dependent term, leaving the isothermal enthalpy change $dH_{T=const}$ with the other two contributions, which is the latent heat dL:

$$dT = \frac{1}{\bar{c}_p}\left(\dot{q}dt - \frac{1}{V}\int_V \sum_\alpha \left(\phi_\alpha \sum_k \frac{\partial H_\alpha}{\partial c_k} dc_k + H_\alpha d\phi_\alpha \right) dV \right) = \frac{1}{\bar{c}_p}(\dot{q}dt - dL) \tag{6}$$

with $\bar{c}_p = \frac{1}{V}\int_V \sum_\alpha c_{p,\alpha}\phi_\alpha dV$.

In the explicit scheme, the latent heat contribution dL attributed to the temperature change dT can be calculated from the corresponding enthalpy change dH and the temperature change dT' and average heat capacity $\bar{c}'_p$ of the previous time step, leading to the expression:

$$dL = dH - \bar{c}'_p dT' \tag{7}$$

This explicit method for solving the temperature change in the simulation domain is quite simple but has the disadvantage of introducing an additional stability criterion: If the enthalpy change with temperature dH/dT is too abrupt, fluctuations can occur while solving Eq. (6). Fortunately, the coupling to the phase-field method introduces a strong kinetic damping which prevents such problems (see also Section 4.1).

The DTA approximation was first proposed by Maxwell and Hellawell [22]. It has been furthermore used in a statistical model for the prediction of the grain size [23] and in phase-field simulation of equiaxed growth [24–26].

3.3. The self-consistent homoenthalpic approximation for simulation of equiaxed solidification

Both approximations described above show deficiencies if applied to equiaxed technical processes. The DTA approximation does not account for thermal interactions between regions with different temperature level, leading to unrealistic temperature–time profiles with exaggerated recalescence. The Bridgman approximation, using a prescribed temperature–time curve, introduces the risk of "violating" microstructure formation if the temperature gradient is not large enough: If release of latent heat (e.g. due to the formation of the primary phase or a eutectic reaction) is not in line with the prescribed temperature–time curve, the approximation may lead to wrong or even numerically instable results.

According to the last statement one can argue that consistency between the local temperature–time curve and morphology formation must be a primary goal to be achieved by a suitable approximation of the general micro–macro problem. This consistency is not fulfilled for the Bridgman approach, but for the DTA approximation, which is one reason why the latter method has been used for simulation of equiaxed solidification [24]. But the exaggerated recalescence produced by this assumption can lead to unrealistic phase sequences, if other phases appear in this temperature range.

This leads directly to an iterative approach to the problem: If the outcome of the microstructure simulation is used as an "improved" description for latent heat release in the macroscopic simulation, self-consistency between microstructure and the temperature–time behavior can be achieved in a few iterations. But this approach assumes that the description of latent heat release is the same all over the casting, even if the local cooling rates are different in different zones of the macroscopic geometry. This is equivalent to the assumption that the average enthalpy relation

$$H(T^{\mathrm{avg}}) = \frac{1}{V_C}\int_{V_C}\sum_{\alpha} H_\alpha(T(x))\phi_\alpha \, dV \tag{8}$$

is uniform within the casting, which in the following will be called "homoenthalpic" approximation. The control volume V_C is a "representative" part of the microstructure simulation domain in which the temperature $T(x)$ is assumed to be close to its average temperature T^{avg}. This point is further discussed in Section 4.2.

4. Phase-field with homoenthalpic coupling to a macroscale temperature solver

For the iterative solution of the general micro–macro problem using the self-consistent homoenthalpic approximation, two transport equations have to be solved on two different length scales:

(1) The temperature equation is solved on the whole casting geometry. Because of the high diffusion length for heat, a relatively coarse grid can be used. Latent heat release is included as a function of temperature using tabulated values for the average enthalpy $H(T)$, heat capacity $C_p(T)$ and conductivity $\lambda(T)$. These values are obtained from the previous microscale results.
(2) The phase transformation and solute diffusion is calculated on the microscale using a fine grid, according to the lower solute diffusion length. The temperature distribution, which is the main driving force for solidification, is taken from the previous results on the macroscale. This is the only information which is transferred from the macroscale to the microscale.

In principle, this type of coupling can be performed using two different software packages, if the macroscopic software allows for a reading in of the tabulated data produced by the microscopic tool.

4.1. Phase-field with an integrated 1D temperature solver

For the self-consistent homoenthalpic approximation, a simplified 1D macro model is used, which is integrated into the phase-field software. The 1D approximation corresponds to a one-dimensional plate geometry, as illustrated in Fig. 1. Alternatively, spherical or cylinder coordinates could be used for corresponding geometries.

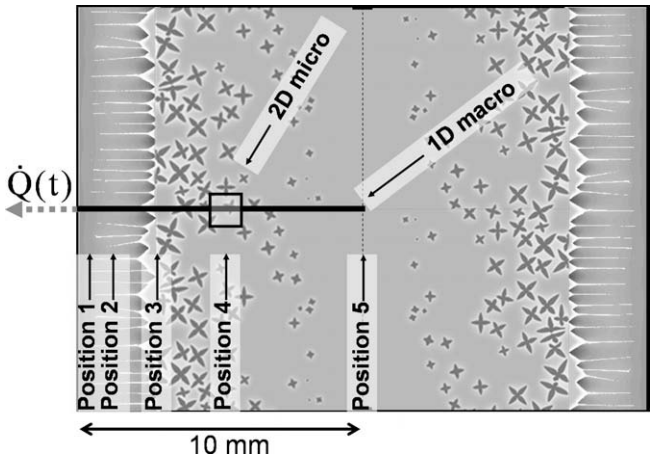

Fig. 1. Plate geometry with rectangular microscopic domain and 1D temperature field. The positions of the micro-domain for which simulations have been performed are pictured.

The 2D microstructure simulation domain is chosen to be "on top of" the 1D temperature field with the ordinate oriented parallel to the temperature gradient. This geometry permits to study also the effect of the temperature gradient on microstructure formation. To allow a more general use of this integrated temperature solver, direct release of latent heat from the micro-simulation domain to the 1D temperature field is implemented, although this would not be necessary for the iterative homoenthalpic approach presented in this paper. Because partly overlapping zones may exist (grid cells in the 1D temperature field which partly receive latent heat from the micro-domain and partly approximated by tabulated data), compatible numerical methods have to be used for both, the parts where the micro-simulation domain is overlapping the temperature field and the rest of the 1D temperature domain. Consequently, the temperature equation for the simplified 1D macro model is derived in analogy to Eq. (6), taking the release of latent heat in the volume V of one macroscopic grid point with the length Δx into account:

$$dT = \frac{1}{\bar{c}_p}\left(\lambda\frac{d^2T}{dx^2}dt - \frac{1}{V}\int_V \sum_\alpha \left(\phi_\alpha \sum_k \frac{\partial H_\alpha \partial c_k dc_k}{+} H_\alpha d\phi_\alpha\right) dV\right) = \frac{1}{\bar{c}_p}\left(\lambda\frac{d^2T}{dx^2}dt - dL\right) \tag{9}$$

with $\bar{c}_p = \frac{1}{V}\int_V \sum_\alpha c_{p,\alpha}\phi_\alpha dV$

Eq. (9) is solved on the whole 1D temperature grid. Depending on whether the position lies inside or outside of the micro-domain, either tabulated data for $H(T), c_p(T)$ and the local heat conductivity $\lambda(T)$ are used or the corresponding values are evaluated from the actual simulation microstructure. In the latter case, in order to reduce the calculation time, these variables, which have to be calculated each time step from the database via the TQ interface, are obtained using the average phase composition, phase fractions and temperature in each volume V of the micro-domain corresponding to one temperature grid cell. For the total enthalpy change in the current time step dH, this is

$$dH = \sum_\alpha d(\bar{\phi}_\alpha H_\alpha), \tag{10}$$

where $\bar{\phi}_\alpha$ is the average phase fraction and H_α the average enthalpy of phase α in the volume V.

The temperature-independent enthalpy change dL can then be calculated using dH and the temperature change dT' as well as the average heat capacity from the previous time step as derived in Section 3.2:

$$dL = dH - \bar{c}'_p\, dT' \tag{11}$$

Eqs. (9) and (11) lead to the final expression for the calculation of the temperature change dT inside the volume V:

$$dT = \frac{1}{\bar{c}_p}\left(\lambda\frac{d^2T}{dx^2}dt - dH + \bar{c}'_p\, dT'\right) \tag{12}$$

As already mentioned in Section 3.2, the explicit solution of the differential Eq. (12) can lead to numerical instabilities if the tabulated $H(T)$ curve is too steep. Other than in the micro-simulation domain where the phase-field and diffusion kinetics provide an effective damping, in the 1D temperature field latent heat release would be instantaneous. Therefore, an artificial kinetic equation is introduced which slightly delays the latent heat release. The effectively realized enthalpy change per time step is calculated as

$$dH^{eff} = k\Delta H^{acc} \tag{13}$$

with ΔH^{acc} being the locally accumulated enthalpy change which has not yet been released. The kinetic constant k must be chosen big enough in order not to retard the latent heat release noticeably ($k = 0.01$ works well, considering the much smaller explicit time step of the temperature solver compared to the phase-field time step).

$H(T)$ and $c_p(T)$ as well as the local heat conductivity $\lambda(T)$ are unknown for the first iteration of the self-consistent homo-enthalpic approach. Tabulated initial data can be created from previous simulation runs or, as done in this paper, using the Scheil approximation.

4.2. The choice of the control volume V_C

Because the ordinate of the 2D micro-simulation domain is oriented parallel to the temperature field, there is a temperature difference between the bottom and the top which depends on the size of the control volume V_C. As a consequence, the enthalpy according to Eq. (8) is averaged over this temperature interval, thus smoothening the $H(T)$ curve which is later used in the 1D temperature solver. This, as a consequence, introduces a smearing of the position of latent heat release which is in the order of the size of the control volume itself and should be no serious problem as long as the size of V_C is small compared to the thermal diffusion length.

On the other hand, if the size of the control volume is too small, $H(T)$ would not be representative. In the case of equiaxed solidification, and if a prediction of the average grain size is intended, the number of dendrites inside the considered region must be high enough to be representative, as well for the evaluation of $H(T)$ as for the grain size. Therefore, it is reasonable to use the same dimension for the control volume and the micro-simulation domain, which has been done in this paper. For other applications like columnar growth, the control volume should be chosen to be smaller than the microstructure simulation domain.

5. Model validation by comparison to other approximations

In the following, the new approach is compared to the Bridgman and DTA approximations which have been alternatively used for simulation of equiaxed solidification and which are described in Section 3. As an example, a hypothetical plate casting of the binary alloy Al–3at%Cu was selected which, during solidification, shows an equiaxed dendritic primary structure of fcc aluminum as well as a eutectic intermetallic Al_2Cu phase. As will be shown, the average grain size is very sensitive to the interaction of the microscopic latent heat formation with the macroscopic heat fluxes. Therefore, the different behavior of the three models can be clearly demonstrated and discussed.

5.1. Simulation procedure

All microstructure simulations are performed on a finite differences grid consisting of 1000×1000 cells with a spatial resolution of 0.5 μm. Periodic boundary conditions are applied for the phase-fields and solute diffusion in x direction, while in y direction (the direction of the temperature gradient) isolating conditions are chosen.. At the beginning, the potential nucleation sites are randomly distributed over the domain, according to an assumed seed density distribution (throughout Section 5, inoculation case B in Fig. 8 is used), and attributed with a critical nucleation undercooling determined by the nucleant size [23]. If this critical undercooling is reached locally, one fcc grain with random orientation is set to this location. At lower temperatures, Al_2Cu seeds are allowed to form on the fcc–liquid interface at a critical undercooling of 10 K. Although the Al_2Cu particles cannot be completely resolved at the given grid spacing, the amount of latent heat related to this reaction is predicted correctly. For a proper description of the thermodynamic properties and the diffusion coefficients the TTAl5 [15] and the MOBAL [14] database are used.

The 1D temperature field consists of 100 grid cells with a size of 100 μm. This corresponds to a plate geometry thickness of 20 mm taking mirror symmetry into account. While in the center of the casting an isolation boundary condition is applied, heat transfer through the surface of the plate is described with a constant heat transfer coefficient of 0.15 $Wcm^{-2}\,K^{-1}$ for the dye with air contact to a temperature of 25 °C. This can be considered as typical conditions for die casting.

Simulations are performed for the different positions 1–5, located at 0.5, 1.0, 2.5, 5.0 and 10.0 mm distance from the plate surface (Fig. 1). Approximated starting curves for $H(T)$, $Cp(T)$ and $\lambda(T)$ are obtained using the Thermo-Calc Scheil model [13]. A thermal conductivity of 0.7 $Wcm^{-1}\,K^{-1}$ is assumed for the melt and 1.4 $Wcm^{-1}\,K^{-1}$ for the solid phases. Linear interpolation is used in the semisolid region. For each position, an iterative solution is obtained starting from the Scheil data and repeatedly replacing the $H(T)$, $Cp(T)$ and $\lambda(T)$ curves by those evaluated inside the micro-domain. Convergence is achieved after 3–4 iterations leading to a self-consistent solution.

The Cu segregation pattern in the micro-domain after 3.0 s and after complete solidification is represented in Fig. 2 for position 4 (Fig. 1). One can see the equiaxed dendrites (left) and the grain structure with the bright eutectic regions (right).

5.2. Comparison to the Bridgman approximation

The term "Bridgman Approximation" generally implies the use of externally obtained temperature–time profiles (cf. Section 3.1). These profiles may be not consistent with microstructure formation if the thermal conditions are far from those in a Bridgman furnace where cooling is slow and the temperature gradient is strong.

In this paper, "Bridgman Approximation" refers to the use of the Scheil model for the pre-calculation of the macroscopic temperature field like it is done in many macroscopic software tools for casting simulation. At the same time, these temper-

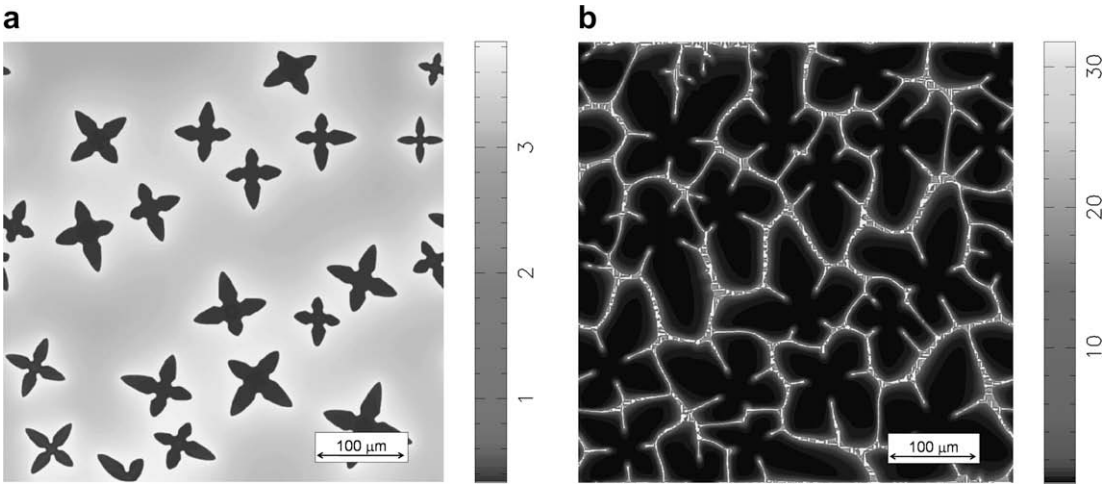

Fig. 2. Cu concentration distributions in the micro-domain at 3.0 s (left) and after complete solidification (right) in at%.

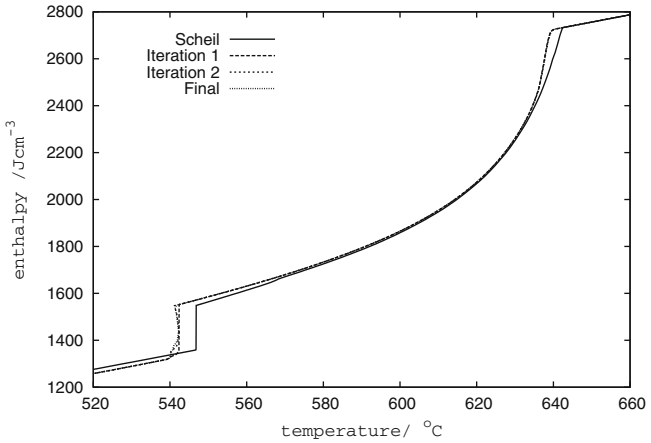

Fig. 3. $H(T)$ curve for different iteration steps at position 4. Shown are the initial Scheil approximation, the first two iterations results and the final solution.

ature–time profiles obtained using the Scheil approximation are used as starting point for iteration in the homoenthalpic approach.

Fig. 3 shows how the enthalpy curve $H(T)$ is changing during the first iterations of the homoenthalpic approach starting from the Scheil approximation. The main differences of the final solution (= self-consistent homoenthalpic approximation) with respect to the initial Scheil curve (= Bridgman approximation) are visible around 640 °C and 545 °C where the formation of the fcc and the Al_2Cu phase, respectively, are observed. The Scheil model leads to a temperature curve which, especially around theses temperatures, is not consistent with microstructure formation. This is most striking near the center of the casting, where the temperature gradient and thus the drain of latent heat is small.

As assumed in the homoenthalpic approximation, the iterations should lead to the same $H(T)$ curve for different positions in the casting. Fig. 4 shows the final curves for all positions which are fairly close to each other but quite far from the Scheil curve. This difference between the homoenthalpic and the Scheil approximation leads to a different temperature–time relation and consequently to a different grain structure (Fig. 5).

5.3. Comparison to DTA approach

The DTA approach has been used for the prediction of the grain size [23] and for the simulation of equiaxed growth morphologies [24–26]. To allow a comparison with the new approach at position 1, a constant heat extraction rate of 83 $Jcm^{-3}\,K^{-1}$ was chosen in order to achieve the same local solidification time as for the homoenthalpic approach (measured between the first appearance of the fcc phase and the onset of the eutectic reaction). No further thermal boundary conditions are needed for the DTA approach, coupling to an external 1D temperature field was disabled.

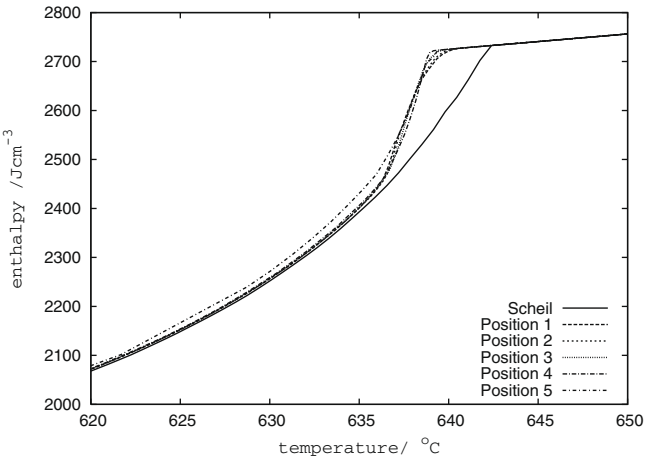

Fig. 4. Final $H(T)$ curves for the different positions. The $H(T)$ curve corresponding to the initial Scheil approximation is included for comparison.

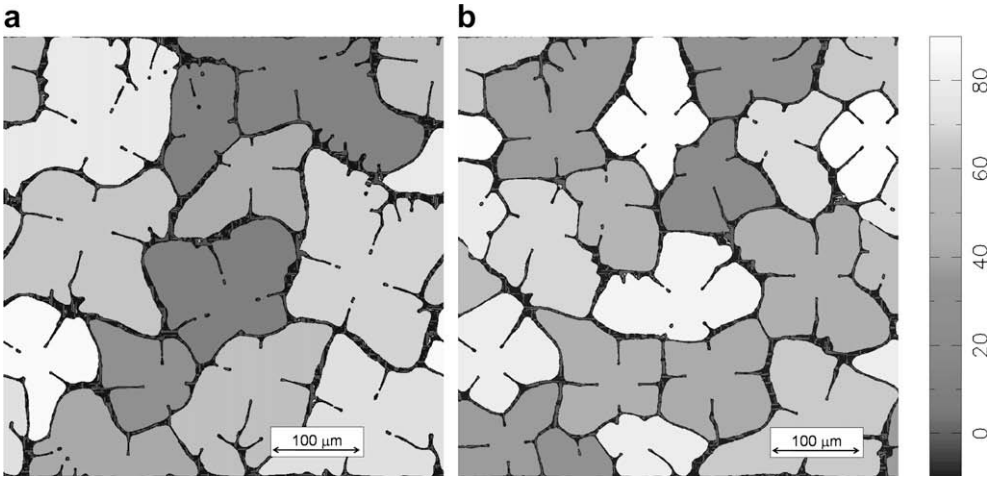

Fig. 5. Comparison of the microstructures after complete solidification, shown as grain orientation maps (orientation angles in degrees). The final solution (left) exhibits a considerably bigger grain size than the results from the Scheil approximation (right side).

Fig. 6 shows the temperature–time curves for both approximations. For comparison, the curves have been shifted in time in such a way that the first appearance of fcc coincides for both curves. It can be clearly seen that the shapes of the curves deviate tremendously: The curve related to the DTA conditions shows pronounced flat zones and recalescence in the temperature regions around 640 and 545 °C (recalescence around 640 °C is small and therefore invisible in Fig. 6). By contrast, the curve related to the new approach shows only slightly flattened regions, much more resembling the typical experimental temperature–time curves in castings. Furthermore, at least far from the center of the casting, the local cooling rate is increasing in time for the DTA case, while for the homoenthalpic case it is relatively constant.

To understand theses striking differences one should remember that the DTA approach is completely neglecting thermal gradients, and only a constant heat extraction rate is used as thermal boundary condition of the micro-simulation domain. A sudden and strong release of latent heat automatically raises the temperature level until the elevated temperature slows down the further heat production, thus leading to the flattened regions in the temperature–time curves. In the case of the homoenthalpic approach, however, heat conduction between the neighboring cells of the 1D temperature field strongly reduces the effect of the local latent heat release and thus decreases the tendency for recalescence or flat regions in the temperature–time curve.

The differences between the two temperature–time curves in Fig. 6 have a strong influence on microstructure, especially on the grain size. Fig. 7 shows the microstructure after solidification. Due to the faster temperature drop around the nucleation temperature, a remarkably smaller grain size and a slightly more dendritic growth morphology can be observed in the case of the self-consistent homoenthalpic approximation.

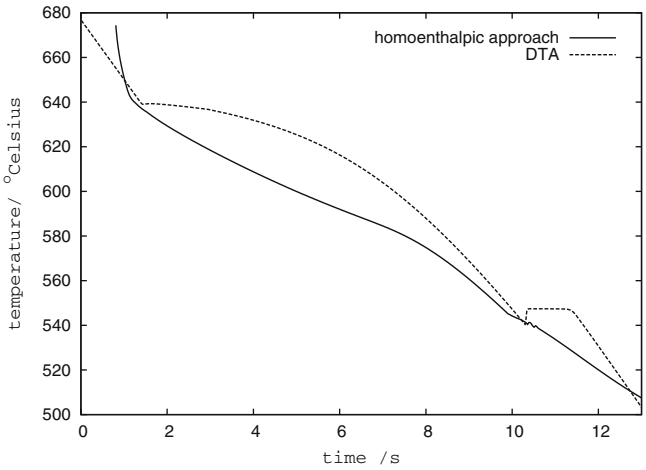

Fig. 6. Comparison of the temperature–time curves for the homoenthalpic and the DTA approach (position 1).

5.4. Discussion

As could be shown in Sections 5.2 and 5.3, the Bridgman and DTA approximation show strong differences to the self-consistent homoenthalpic approach regarding the resulting temperature–time curves and microstructures. These differences were explained by the specific deficiencies of the two models.

The similarity of the $H(T)$ curves for different positions in the casting (Fig. 4) is a strong indication that the self-consistent homoenthalpic approach is working quite well in this case, at least when compared to the other approximations. This could be not the case if strong kinetic effects like a strongly rate dependent nucleation behavior or a morphological change between different zones in the casting were present. Then, the basic assumption of a common enthalpy–temperature behavior in all zones of the casting would not be valid any more.

But even though the method turned out to perform better than the Bridgman and DTA approximation, the question has to be posed whether there is still room for improvements. As already discussed in Section 4.2, a critical point of this method is the choice of the control volume V_C, which, according to Eq. (8), determines the temperature interval over which the enthalpy is averaged. If V_C was chosen too big, a smearing of the $H(T)$ relation, especially for the positions near the edge of the casting, would have to be expected. Effectively, looking at Fig. 4, this effect seems to play a role in the present example: especially for position 1 in the casting, the kink which corresponds to the beginning formation of the fcc phase appears smoother than for position 5. Indeed, the temperature profiles around this temperature show a thermal gradient which covers the range of nearly zero for position 5 and around 80 K/cm for position 1, corresponding to a temperature difference of up to 4 K between the bottom and the top of the control volume. This artifact could be reduced by choosing a smaller control volume for the outer positions (which would still be representative in this case keeping in mind the higher density of grains, see

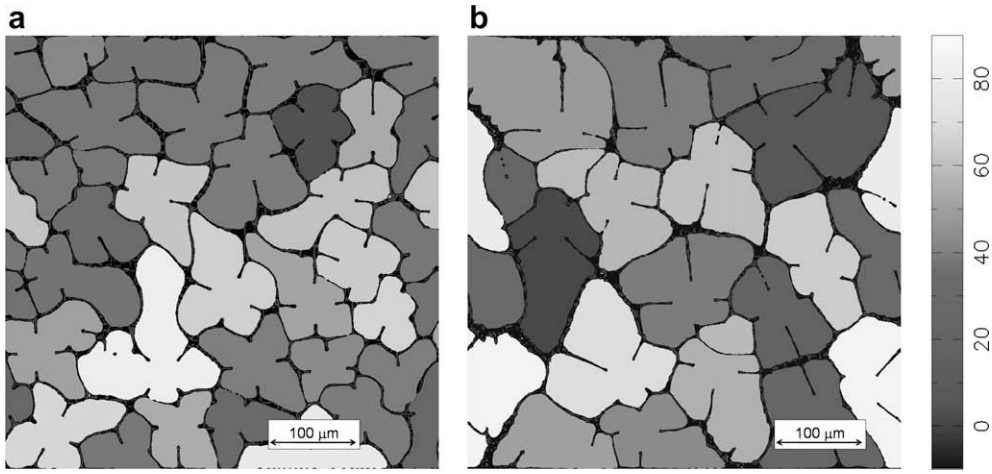

Fig. 7. Comparison of the resulting grain structures for the homoenthalpic approach (left) and the DTA approach (right) for the simulations in Fig. 6 (orientation in degrees).

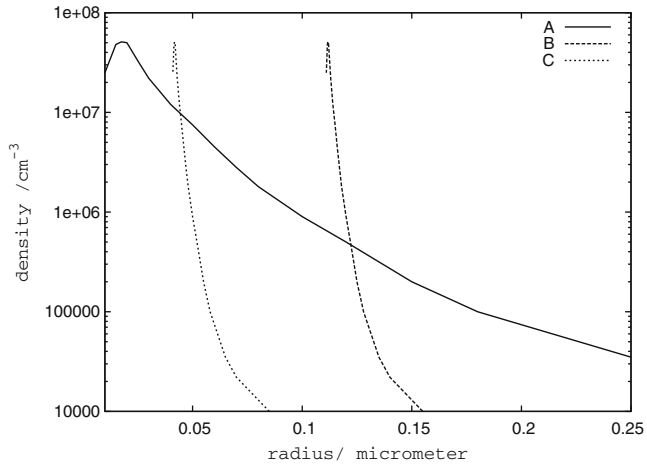

Fig. 8. Three different inoculation scenarios (A–C), given in form of radius-seed density curves.

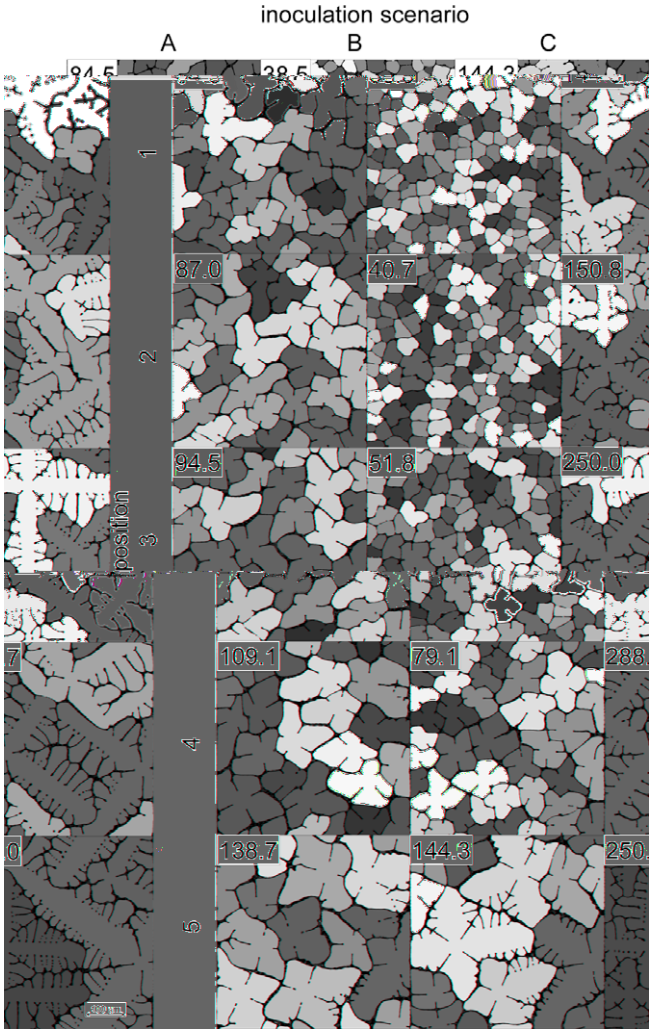

Fig. 9. Compilation of the grain structures for all five positions and all three inoculation scenarios. For each combination, the grain orientation maps (orientation in degrees) and the values of the average grain size are given for the final iteration.

Fig. 9, inoculation scenario B) or by aligning the microstructure simulation domain perpendicular to the temperature gradient.

6. Application to the simulation of grain structures in an equiaxed Al–3at%Cu casting

In technical aluminum castings, inoculation plays an important role for the reduction of the grain size. Grain refinement strongly depends on the shape of the seed density distribution. Phase-field simulation delivers important information not only on grain sizes but also on the grain morphologies.

In the following, the homoenthalpic approach is applied to the equiaxed solidification of Al–3at%Cu, using three hypothetical seed density distribution curves A–C (Fig. 8) and following the simulation procedure explained in Section 5.1. While the seed density distribution A covers a wide range of nucleant radii, B and C are given a corresponding but much steeper shape. Additionally, C is shifted to smaller radii, i.e. it exhibits a smaller average radius compared to B (cf. Fig. 8). This allows for investigating the general effect of the seed density distribution on the grain size and its distribution on the casting, and also exemplarily demonstrates the capabilities of the phase-field method together with the iterative homoenthalpic approach.

Fig. 9 resumes all simulations done for the three different inoculation scenarios and for all five positions in the casting. The resulting average grain size (calculated from the average area occupied by one grain) is inserted into the individual grain structure representations in Fig. 9. The most striking difference can be seen if we compare the results for the distributions B and C: shifting the curve to higher radii obviously reduces the average grain size. This can be explained by the lower undercooling at which the nuclei are formed. The lower growth rate and the resulting slower latent heat production leads to the activation of a higher number of nuclei.

Compared to B and C, the relatively flat distribution A produces intermediate grain sizes. But interestingly, the variation of the average grain size over the casting is much smaller in comparison to the steep distributions B and C. This can also be understood in terms of the distribution of the critical undercooling: If the radius distribution of the seeding particles is relatively flat, a considerable increase in undercooling would be needed to notably increase the number of activated nuclei. Hence, the dependency of the grain size on the local cooling rate, and, herewith, on the position in the casting, is much smaller for case A than for B and C.

The results in Fig. 9 also allow for comparing grain morphologies for the different conditions. The tendency for the formation of dendrite side branches depends on both the grain size and the local thermal conditions. Especially in the cases where strong cooling is combined with big grain size, a very dendritic morphology can be observed, as for the inoculation case C. For a given inoculation situation, the tendency for the formation of side branches may increase with grain size if there is a strong dependency of the grain size on the cooling rate. This is especially the case for the steep distribution B. For very flat distributions, even flatter than A, a reversed dependency should be observed. This should be checked in the future by simulations using more seed density distribution variants.

7. Summary

A self-consistent homoenthalpic approach for microstructure simulation of equiaxed solidification in technical castings has been proposed. The approach is based on the postulation of a universal enthalpy–temperature relation $H(T)$ which is assumed to be valid for the whole casting and which is self-consistently derived by microstructure simulation. It allows for consistently coupling of the macroscopic heat balance to the microscopic latent heat production without the necessity to perform microstructure simulations on the whole casting.

A comparison to the Bridgman and DTA approach, which have been widely used in the past, revealed that the new method leads to much more realistic temperature–time curves than the DTA approach, and at the same time avoids the risk of "violating" microstructure formation, which can be the case for externally obtained non-consistent temperature–time profiles applied as thermal boundary condition to the microstructure simulation ("Bridgman" approach). As a consequence, the homoenthalpic approach, when compared to the other methods, leads to different results for the average grain size and morphology which are assumed to be more realistic. A direct experimental validation of these findings unfortunately is difficult as an exact knowledge of the underlying seed density distribution would be needed.

Furthermore, three hypothetical inoculation case scenarios have been investigated in order to study the practical applicability of the new approach. It can be concluded that the computational effort of the self-consistent homoenthalpic approach is acceptable as convergence typically was achieved after only three iterations. For the application case it was shown that the microstructure and its distribution over the casting as well as the self-consistent $H(T)$ relation depend strongly on inoculation. When comparing the results of the microstructure simulation for the three inoculation case scenarios and the different positions in the casting, the specific differences could be explained in terms of the different shapes of the corresponding seed density distributions.

In conclusion, it could be demonstrated by means of the simulation results in this paper and theoretical arguments, that the new approach is very powerful, especially for the conditions of technical equiaxed castings, while the alternative approaches ("Bridgman Approximation" or "DTA" approximation") should be used only for the corresponding thermal conditions (Bridgman and DTA experiment, respectively). The approach equally allows for the use of more advanced macroscopic casting simulation tools if those are able to use $H(T)$ curves for the description of latent heat.

The limits of the method are situations which are strongly determined by interface kinetics, or if a considerable part of columnar regions is involved and the prediction of the columnar-to-equiaxed transition (CET) is crucial. In these cases, more advanced techniques which use different enthalpy curves for different morphological regions should be applied.

Acknowledgment

The author would like to thank the German Research Foundation (DFG) for their support within the Cluster of Excellence "Integrative Production Technology for High-Wage Countries".

References

[1] G. Guillemot, Ch.A. Gandin, H. Combeau, R. Heringer, A new cellular automaton-finite element coupling scheme for alloy solidification, Model. Simul. Mater. Sci. Eng. 12 (2003) 545–556.
[2] Ch.A. Gandin, M. Rappaz, A 3D cellular automaton algorithm for the prediction of dendritic grain growth, Acta Mater. 45 (1997) 2187–2195.
[3] C.Y. Wang, C. Beckermann, Prediction of columnar to equiaxed transition during diffusion-controlled dendritic alloy solidification, Met. Trans. 25A (1994) 1081–1093.
[4] B. Pustal, B. Böttger, A. Ludwig, P.R. Sahm, A. Bührig-Polaczek, Simulation of macroscopic solidification with an incorporated one-dimensional microsegregation model coupled to thermodynamic software, Metall. Mater. Trans. B 34 (2003) 411–419.
[5] J. Tiaden, B. Nestler, H.J. Diepers, I. Steinbach, The multiphase-field model with an integrated concept for modelling solute diffusion, Physica D 115 (1998) 73–86.
[6] A.A. Wheeler, W.J. Boettinger, G.B. Mc Fadden, A phase-field model of solute trapping during solidification, Phys. Rev. E 47 (1993) 1893–1909.
[7] S.G. Kim, W.T. Kim, T. Suzuki, Phase-field model for binary alloys, Phys. Rev. E 60 (1999) 7186–7197.
[8] J. Eiken, B. Böttger, I. Steinbach, Multiphase-field approach for multicomponent alloys with extrapolation scheme for numerical application, Phys. Rev. E 73 (2006) 066122.
[9] M. Plapp, Three-dimensional phase-field simulations of directional solidification, J. Crystal Growth 303 (2007) 49–57.
[10] J.C. Ramirez, C. Beckermann, Examination of binary alloy free dendritic growth theories with a phase-field model, Acta Mater. 53 (2005) 1721–1736.
[11] http://www.micress.de.
[12] I. Steinbach, F. Pezzolla, B. Nestler, M. Seeßelberg, R. Prieler, G.J. Schmitz, J.L. L Rezende, A phase field concept for multiphase systems, Physica D 94 (1996) 135–147.
[13] http://www.thermocalc.com.
[14] MOBAL, http://www.thermocalc.com.
[15] TTAl5, http://www.sentesoftware.co.uk.
[16] B. Böttger, M. Apel, J. Eiken, P. Schaffnit, I. Steinbach, Phase-field simulation of solidification and solid-state transformations in multicomponent steels, Steel Res. Int. 79 (8) (2008) 608–616.
[17] C. Eck, P. Knabner, S. Korotov, A two-scale method for the computation of solid–liquid phase transitions with dendritic microstructure, J. Comput. Phys. 178 (2002) 58–80.
[18] A. Badillo, C. Beckermann, Phase-field simulation of the columnar-to-equiaxed transition in alloy solidification, Acta Mater. 54 (2006) 2015–2026.
[19] H.B. Dong, P.D. Lee, Simulation of the columnar-to-equiaxed transition in directionally solidified Al–Cu alloys, Acta Mater. 53 (2005) 659–668.
[20] J. Li, J. Wang, G. Yang, Phase-field simulation of microstructure development involving nucleation and crystallographic orientations in alloy solidification, J. Crystal Growth 309 (2007) 65–69.
[21] L. Tan, N. Zabaras, Modeling the growth and interaction of multiple dendrites in solidification using a level set method, J. Comput. Phys. 226 (2007) 131–155.
[22] I. Maxwell, A. Hellawell, A simple model for grain refinement during solidification, Acta Metall. 23 (1975) 229–237.
[23] T.E. Quested, A.L. Greer, Grain refinement of Al alloys: mechanisms determining as-cast grain size in directional solidification, Acta Mater. 52 (2004) 3859–3868.
[24] B. Böttger, J. Eiken, I. Steinbach, Phase field simulation of equiaxed solidification in technical alloys, Acta Mater. 54 (2006) 2697–2704.
[25] B. Böttger, J. Eiken, M. Ohno, G. Klaus, M. Fehlbier, R. Schmid-Fetzer, I. Steinbach, A. Bührig-Polaczek, Controlling microstructure in magnesium alloys: a combined thermodynamic, experimental and simulation approach, Adv. Eng. Mater. 8 (2006) 241–247.
[26] J. Eiken, B. Böttger, I. Steinbach, in: Proceedings of the Fifth Decennial International Conference on Solidification Processing SP07, Sheffield, 23–25 July, 2007, pp. 148–152.